Materials Advances

ROYAL SOCIETY OF CHEMISTRY

PAPER

View Article Online
View Journal | View Issue

Check for updates

Cite this: *Mater. Adv.*, 2024, 5, 7222

Preparation of $Li_{2+x}In_xZn_{1-x}Cl_{4+2x}$ ($0 \leq x \leq 0.5$) solid electrolyte and its application in all-solid-state Li-ion batteries

Nguyen Thi Minh Nguyet,[ab] Tran Viet Toan,[bc] Luu Tuan Anh,[bc] Luong Thi Quynh Anh,[bc] Tran Anh Tu[abc] and Nguyen Huu Huy Phuc *[abc]

Received 18th April 2024,
Accepted 7th August 2024

DOI: 10.1039/d4ma00405a

rsc.li/materials-advances

$Li_{2+x}In_xZn_{1-x}Cl_{4+2x}$ ($0 \leq x \leq 0.5$) solid electrolytes were synthesized using a mechanochemical method. XRD indicated that the prepared samples had a cubic structure. The lattice parameter was dependent on the value of x. The cold-pressed pellet of the sample with $x = 0.45$ had an ionic conductivity of about 2.4×10^{-4} S cm^{-1} at 25 °C and an activation energy of about 0.446 eV. The equivalence circuit and distribution of the relaxation time indicated that grain boundary resistance was the main component of the total resistance of the sample. The hot-pressed pellet of the sample with $x = 0.45$ had an ionic conductivity of about 9.2×10^{-4} S cm^{-1} at 25 °C and an activation energy of about 0.300 eV, which were comparable with those of the reported halide-based solid electrolyte. The solid-state cell employing the sample with $x = 0.45$ as a solid electrolyte and bare $LiNi_{0.5}Mn_{0.3}Co_{0.2}O_2$ as the active material showed good cyclic ability at room temperature.

Open Access Article. Published on 07 August 2024. Downloaded on 2/5/2026 10:04:04 AM.
This article is licensed under a Creative Commons Attribution-NonCommercial 3.0 Unported Licence.

1. Introduction

All-solid-state Li-ion batteries (ASS LIBs) have been investigated for a long time, and have been intensively studied from about 2010. At its most basic, an all-solid battery uses a solid electrolyte instead of an electrolyte solution. Replacement of an electrolyte solution by a solid electrolyte could make an all-solid battery able to operate at high temperatures and have a higher energy density than conventional batteries.[1] The solid electrolyte is the most important component when moving from a conventional LIB to an ASS LIB. Solid electrolytes can be divided into the following groups: oxides, sulfides, hydrides, halides and polymers.[2]

The biggest disadvantage of an oxide solid electrolyte is the very high sintering temperature, about 1000 °C, to bind the oxide particles. Meanwhile, the inter-particle adhesion of halide and sulfide solid electrolytes can take place under medium pressure (about 100–700 MPa) and room temperature. This is a huge advantage when applied to mass production. The sulfide solid electrolyte is unstable when in contact with the positive electrode active material that has a voltage greater than 2.80 V *vs.* Li/Li$^+$; therefore, it is necessary to create a thin film to separate the active material and the sulfidic solid electrolyte to prevent the reaction between the two materials.[3] In contrast, halide electrolytes (F^-, Cl^-, Br^-) are stable at high voltages, making them suitable for use in the positive electrode of ASS LIBs.

Halide solid electrolytes were studied in the early 1930s with LiI being the typical research object.[4] In 2018, high ionic conductivity Li_3YCl_6/Li_3YBr_6 materials were successfully synthesized and their application in ASS batteries was reported.[5] The synthesis of Li_3InCl_6 using an aqueous solution was first reported in 2019.[6] Since then, several members of this group have been extensively studied and reported.[7,8] The monoclinic Li_2ZrCl_6 prepared at a high temperature exhibited a low Li$^+$ conductivity of 5.7×10^{-6} S cm^{-1}, but the mechano-chemically prepared hexagonal close-packed Li_2ZrCl_6 showed a moderate Li$^+$ conductivity of 4.0×10^{-4} S cm^{-1} at 30 °C.[9] It was reported that the ionic conductivity of monoclinic Li_2ZrCl_6 was improved from 7.1×10^{-6} to 2.1×10^{-3} S cm^{-1} at 30 °C due to the aliovalent substitution of Zr by In.[10] High-energy ball-milling derived Mn^{2+} doped Li_2ZrCl_6 had an ionic conductivity of 8.0×10^{-4} S cm^{-1} at room temperature, which was higher than that of bare Li_2ZrCl_6.[11] The disordered cubic spinel $Li_{1.9}Sc_{0.7}Cl_4$, $Li_{2.08}Sc_{0.64}Cl_4$ and $Li_2Sc_{2/3}Cl_4$ showed high ionic conductivities of 1.09×10^{-3}, 1.22×10^{-3} and 1.5×10^{-3} S cm^{-1}, respectively, at 30 °C.[12] The mechanochemically synthesized $LiAlCl_4$ had a monoclinic structure and exhibited an ionic conductivity of about 2.1×10^{-5} S cm^{-1} at room temperature, which was about 20 times higher than the reported value of the material prepared by solid state reaction at a high temperature.[13]

[a] *VNU-HCM Key Laboratory for Material Technologies, Ho Chi Minh City University of Technology (HCMUT), 268 Ly Thuong Kiet Str., Dist. 10, Ho Chi Minh City, Vietnam. E-mail: nhhphuc@hcmut.edu.vn*
[b] *Vietnam National University Ho Chi Minh City, Linh Trung Ward, Thu Duc Dist., Ho Chi Minh City, Vietnam*
[c] *Faculty of Materials Technology, Ho Chi Minh City University of Technology (HCMUT), 268 Ly Thuong Kiet Str., Dist. 10, Ho Chi Minh City, Vietnam*

© 2024 The Author(s). Published by the Royal Society of Chemistry

Open Access Article. Published on 07 August 2024. Downloaded on 2/5/2026 10:04:04 AM. This article is licensed under a Creative Commons Attribution-NonCommercial 3.0 Unported Licence.

Most of the reported halide solid electrolytes are based on rare earth elements.[14–17] Li_3TiCl_6, $LiAlX_4$ (X = Cl, Br, I) and Li_2ZnCl_4 are the reported solid electrolytes that employed earth-abundant elements.[18–21] Li_2ZnCl_4 had a cubic spinel structure at low temperature and an olivine structure at temperatures higher than 215 °C.[21] The ionic conductivity of olivine Li_2ZnCl_4 was about 2.0×10^{-4} S cm^{-1} at 280 °C. The ionic conductivity of cubic spinel Li_2ZnCl_4 was about 10^{-7} S cm^{-1} at 100 °C. Therefore, the improvement of the ionic conductivity of cubic Li_2ZnCl_4 is an interesting issue. This study aimed to prepare a cubic $Li_{2+x}In_xZn_{1-x}Cl_{4+2x}$ ($0 \leq x \leq 0.5$) solid electrolyte using mechanochemical synthesis. The as-prepared samples were subsequently heat-treated at 170 °C for 4 h in a dry argon atmosphere. The samples had a cubic structure. The resistance of cubic Li_2ZnCl_4 was too large to be measured at room temperature. The ionic conductivity of the sample $Li_{2.45}In_{0.45}Zn_{0.55}Cl_{4.9}$ (x = 0.45, hot-pressed) was about 9.2×10^{-4} S cm^{-1} at 25 °C. The ASS cell employing $Li_{2.45}In_{0.45}Zn_{0.55}Cl_{4.9}$ solid electrolyte and $LiNi_{0.5}Mn_{0.3}Co_{0.2}O_2$ as an active material showed good cyclic ability at room temperature.

2. Experimental

LiCl (99.99% purity; Macklin), $ZnCl_2$ (99.99% purity; Macklin), $InCl_3$ (99.99% purity; Macklin) were purchased and used without further purification. In a typical batch (2 g of raw materials), appropriate amounts of the raw materials were weighed and mixed using a mortar and pestle for about 15 min and then placed in a zirconia pot (45 mL) with 30 g of zirconia balls (∅ 5 mm). The pot was rotated at 360 rpm using a Pulverisette 7 (Fritsch) for 12 h. The obtained samples were recovered and heat treated at 170 °C for 4 h in a dry argon atmosphere.

The structures of the prepared powders were characterized by XRD (Bruker X8) and thermogravimetry–differential thermal analysis (TG–DTA; EVO II, Rigaku). TG–DTA data were obtained in a dry nitrogen flow at a heating rate of 5 K min^{-1}. The total resistivity of the prepared samples was recorded using alternating current impedance spectroscopy (PGSTAT302N, Autolab, Switzerland) from 1 MHz to 10 Hz under a dry N_2 flow. The solid electrolyte pellets were made as previously reported.[22]

$LiNi_{0.5}Mn_{0.3}Co_{0.2}O_2$ (MTI) (hereafter denoted as NCM) without any coating was employed as an active material in an ASS cell to study the stability of the prepared solid electrolyte. The positive electrode composites were prepared by manually mixing NCM, the sample $Li_{2.45}In_{0.45}Zn_{0.55}Cl_{4.9}$ (x = 0.45, heat-treated at 170 °C), and Ketjen Black with a weight ratio of 68.5 : 28.5 : 3.0 using an agate mortar. The ASS cell composed of the prepared electrode composite (about 11.0 mg), Li_6PS_5Cl (about 100 mg) as separator, and a Li–In negative electrode was fabricated using the reported procedure.[23] About 100 mg of Li_6PS_5Cl were pressed in a polycarbonate mold (diameter of 10 mm) under 100 MPa for 1 min. About 11.0 mg of the electrode composite was dispersed on one side of the Li_6PS_5Cl layer and pressed under 330 MPa for 5 min. A piece of In metal foil (Aldrich, 99.995%, 8 mm diameter, 0.1 mm thickness) was placed on the other side of the Li_6PS_5Cl, followed by attaching a piece of Li foil (Aldrich, 99.999%, 4 mm diameter, 0.1 mm thickness) on the In foil. The cell was then pressed at 30 MPa

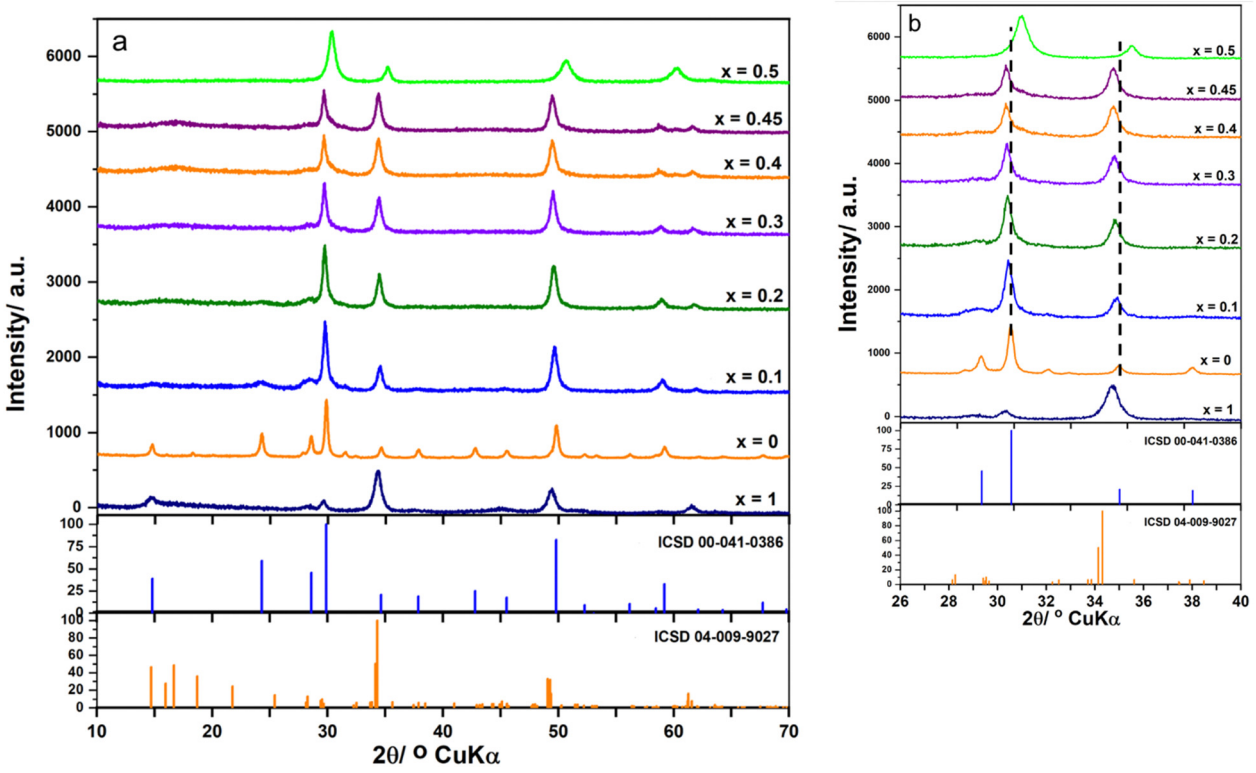

Fig. 1 (a) XRD patterns of the as-prepared $Li_{2+x}In_xZn_{1-x}Cl_{4+2x}$ ($0 \leq x \leq 0.5$) samples; (b) enlargement of Fig. 1a.

Open Access Article. Published on 07 August 2024. Downloaded on 2/5/2026 10:04:04 AM.
This article is licensed under a Creative Commons Attribution-NonCommercial 3.0 Unported Licence.

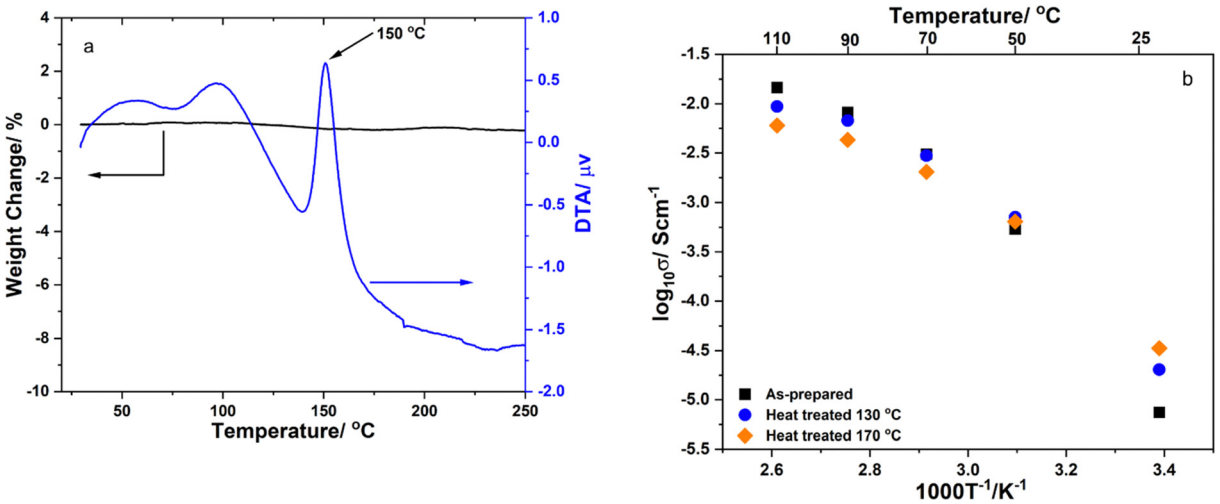

Fig. 2 (a) TG-DTA curves of the $Li_{2.4}In_{0.4}Zn_{0.6}Cl_{4.8}$ sample; (b) temperature dependence of the ionic conductivity of the $Li_{2.4}In_{0.4}Zn_{0.6}Cl_{4.8}$ solid electrolyte heat-treated at different temperatures.

for 30 sec. Stainless-steel rods with a diameter of 10 mm were used as a current collector (electrode area 0.785 cm^2). The cell was rested at room temperature for 2 h before the cycling test. Galvanostatic testing of the cells involved cycles in CC mode (1C = 200 mA h g^{-1}) using a VMP3 (BioLogic) to study the stability of the sample with x = 0.45. The cut-off voltages were 3.70 and 2.40 V *vs.* Li–In. All electrochemical measurements were recorded at room temperature.

All the experiments were carried out in a glove box (Ar-filled, $[H_2O] < 0.1$ ppm) or an airtight sample holder.

3. Results and discussion

Fig. 1 shows the XRD patterns of the as-prepared $Li_{2+x}In_x$-$Zn_{1-x}Cl_{4+2x}$ ($0 \leq x \leq 0.5$) samples, and the standard patterns of Li_2ZnCl_4 and Li_3InCl_6. The peaks of the sample with x = 1 were in agreement with those of Li_3InCl_6 prepared by the high-energy ball-milling method and ICSD card number 04-009-4027.[24] The pattern of the sample with x = 0 (Li_2ZnCl_4) exhibited the formation of a nearly pure cubic spinel phase and is in agreement with ICSD card number 00-041-0386.[12] The samples with x = 0.1, 0.2, 0.3 and 0.4 exhibited similar patterns to that with x = 0. The existence of a new peak at $2\theta \approx 60°$ in the pattern of the sample with x = 0.5 suggested that the structure of this sample was different from that of cubic Li_2ZnCl_4. Fig. 1b shows that the peaks located at $2\theta \approx 30.10$ and 34.89° for x = 0.1, 0.2, 0.3 and 0.4 shifted to the left compared with those for x = 0. Considering that the ionic diameter of In^{3+} is bigger than that of Zn^{2+}, the left shift of those peaks indicated that Zn^{2+} was partly replaced by In^{3+} in the Li_2ZnCl_4 cubic structure. This observation proved that a $Li_{2+x}In_xZn_{1-x}Cl_{4+2x}$ ($x < 0.5$) solid solution was successfully prepared by the high-energy ball-milling method.

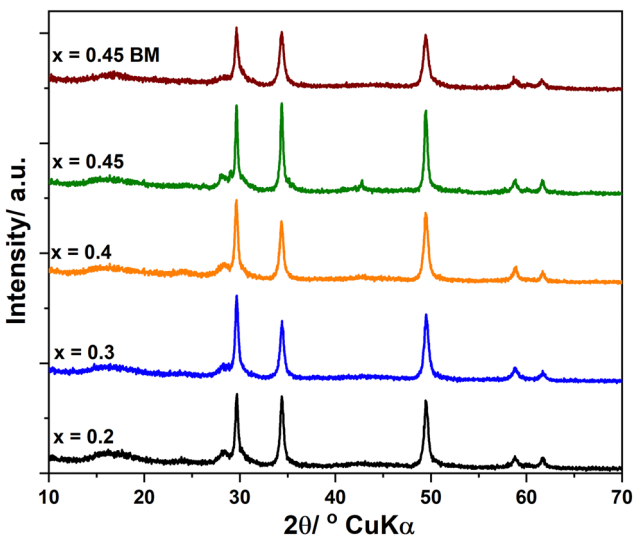

Fig. 3 XRD patterns of $Li_{2+x}In_xZn_{1-x}Cl_{4+2x}$ ($0 \leq x \leq 0.5$) samples after heat-treatment at 170 °C for 4 h and the sample with x = 0.45 after ball milling (x = 0.45 BM).

Fig. 2a illustrates the TG-DTA curves of the $Li_{2.4}In_{0.4}$-$Zn_{0.6}Cl_{4.8}$ sample. The TG curve showed only about 0.1% weight loss due to the desorption of adsorbed water on the sample's surface. There was a small endothermic peak from about 50 °C to 100 °C indicating the elimination of physically adsorbed water molecules. A sharp exothermic peak located at about 150 °C indicated the crystallization of the sample. The peak started at about 140 °C and ended at about 170 °C. Thus, the sample $Li_{2.4}In_{0.4}Zn_{0.6}Cl_{4.8}$ was heated at 130 and 170 °C for 4 h to study the effect of heat treatment on its ionic conductivity at room temperature. The temperature dependence of the ionic conductivity of the $Li_{2.4}In_{0.4}Zn_{0.6}Cl_{4.8}$ solid electrolyte heat-treated at different temperatures is depicted in Fig. 2b. The ionic conductivities at 25 °C of the as-prepared sample, the sample heat treated at 130 °C and the sample heat treated at 170 °C were about 2.0×10^{-5}, 3.2×10^{-5} and 5.6×10^{-5} S cm^{-1}, respectively. Therefore, the other samples were also treated at 170 °C for 4 h.

© 2024 The Author(s). Published by the Royal Society of Chemistry

Open Access Article. Published on 07 August 2024. Downloaded on 2/5/2026 10:04:04 AM.
This article is licensed under a Creative Commons Attribution-NonCommercial 3.0 Unported Licence.

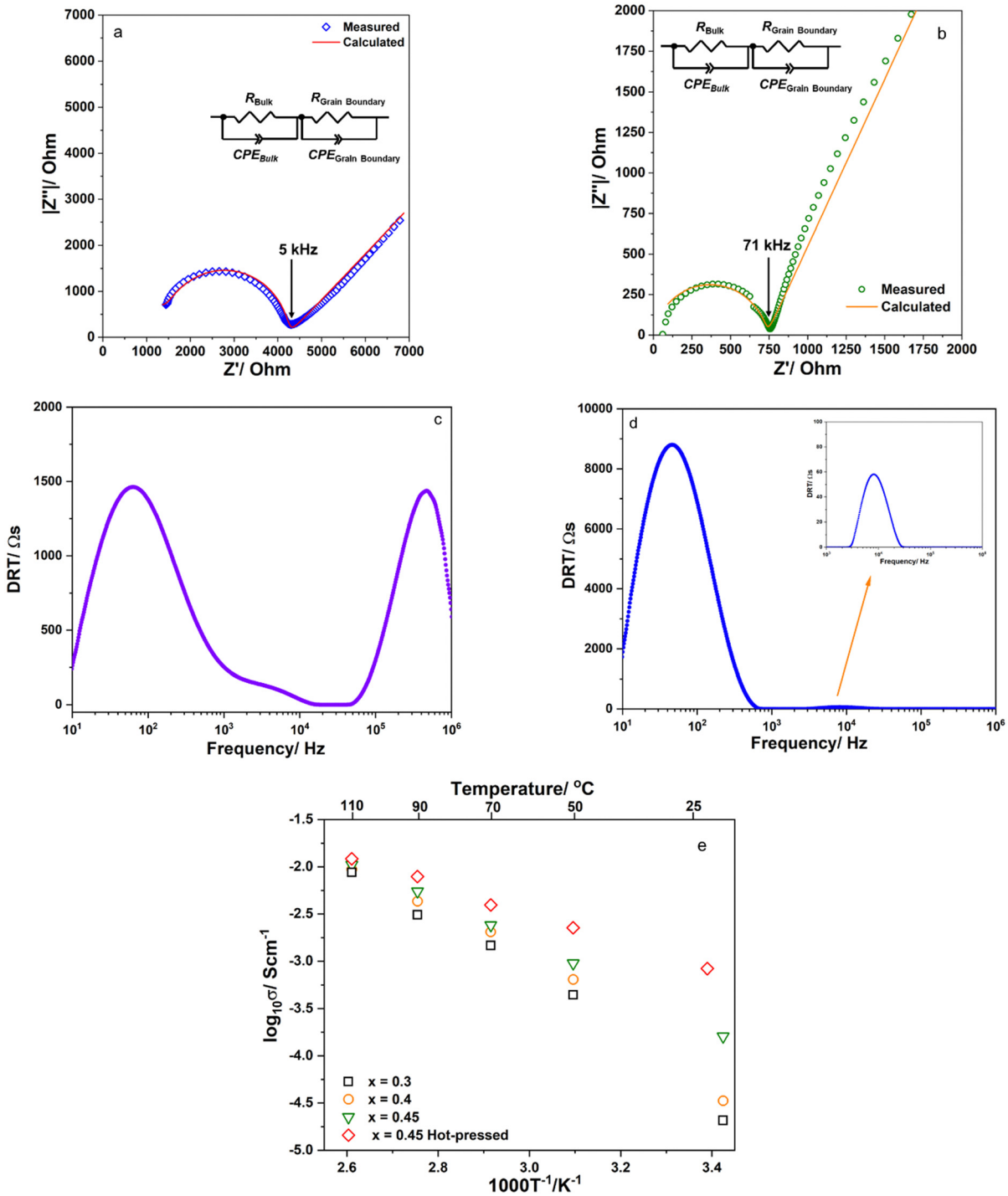

Fig. 4 (a) and (b) Nyquist plots and fitting curves for x = 0.3 and 0.45, respectively. The insets show the equivalence circuits. (c) and (d) The distributions of the relaxation times for x = 0.3 and 0.45, respectively. (e) Temperature dependence of the ionic conductivity for x = 0.3, 0.4 and 0.45 solid electrolytes heat-treated at 170 °C for 4 h.

Fig. 3 shows XRD patterns of $Li_{2+x}In_xZn_{1-x}Cl_{4+2x}$ samples ($0.2 \leq x \leq 0.45$) after heat-treatment at 170 °C for 4 h and the sample with x = 0.45 after ball milling (x = 0.45 BM). The patterns illustrate that the cubic structure of the prepared samples was still preserved after heating at 170 °C. It can be seen that the patterns of the sample with x = 0.45 before and after heat treatment were similar; however, the peaks of the heat-treated sample were sharper than those of the as-prepared sample. This indicated that the crystalline size increased after the heat treatment process. The patterns had three main peaks

Open Access Article. Published on 07 August 2024. Downloaded on 2/5/2026 10:04:04 AM. This article is licensed under a Creative Commons Attribution-NonCommercial 3.0 Unported Licence.

at $2\theta \approx 29.64$, 34.37, 49.49, 58.82 and 61.77°. The lattice parameters were obtained at each diffraction angle θ using the Bragg equation.

$$n\lambda = 2d\sin\theta \quad (1)$$

$$\frac{1}{d_{hkl}{}^2} = \frac{h^2+k^2+l^2}{a^2} \quad (2)$$

The results obtained from (1) and (2) confirmed that the prepared samples had a cubic structure and the mentioned peaks were assigned to the [222], [400], [440], [622] and [444] planes, respectively. The Nelson–Riley equation was employed to determine the lattice parameter a_0:[25]

$$a \approx \frac{1}{2}\left(\frac{\cos\theta^2}{\sin\theta}+\frac{\cos\theta^2}{\theta}\right) \quad (3)$$

a_0 was determined from a linear fit equation, which was derived from a plot with a as the y-axis and $\frac{1}{2}\left(\frac{\cos\theta^2}{\sin\theta}+\frac{\cos\theta^2}{\theta}\right)$ as the x-axis. The obtained lattice parameters for the samples with x = 0.2, 0.3, 0.4 and 0.45 were 10.379, 10.401, 10.425 and 10.45 Å, respectively.

Fig. 4a and b show the Nyquist plots and fitting curves for x = 0.3 and 0.45 recorded at room temperature. The insets show the equivalence circuits. The plots a composed of a semicircle and a low-frequency tail consistent with Li^+ blocking at the stainless-steel electrodes, demonstrating ionic conduction properties. The parallel-plate capacitor model was used to estimate the capacitance C of the grain boundary and bulk:

$$C = \varepsilon_0\varepsilon_r\frac{A}{d} = C_0\varepsilon_r \quad (4)$$

where ε_r is the value of the inflection point in the plot of ε'. The real part of the permittivity, ε', was calculated using the following equation:

$$\varepsilon' = -\frac{Z''}{\omega C_0(Z'^2+Z''^2)}$$

where $C_0 = \varepsilon_0(A/d)$ is the free space capacitance of the cell, ε_0 is the permittivity of free space (8.854×10^{-14} F m^{-1}), and A and d are the surface area and thickness, respectively, of the sample pellet. For the sample with x = 0.3, the capacitance of the grain boundary and bulk were approximately 1.1 nF and 4.7 pF, respectively. For the sample with x = 0.45, the capacitance of the grain boundary and the bulk were approximately 0.6 nF and 1.3 pF, respectively. The resistance components for x = 0.3 and 0.45 were double-checked using the distribution relaxation time (DRT).[26] The results are illustrated in Fig. 4c and d for the samples with x = 0.3 and 0.45. The DRT spectrum for x = 0.3 (Fig. 4c) consists of two peaks located at low (10^3–10^4 Hz) and high frequency (10^5–10^6 Hz) regions, indicating the contribution of the grain boundary and bulk resistance to the ionic conductivity of this sample. The DRT spectrum for x = 0.45 (Fig. 4d) shows the major peak in the low frequency ($\sim10^4$ Hz) region and an almost negligible peak in the high frequency region. Thus, the grain boundary gave rise to the major resistance of this sample. The temperature dependence of the ionic conductivity of the x = 0.3, 0.4 and 0.45 solid electrolytes heat-treated at 170 °C for 4 h are plotted in Fig. 4d. The ionic conductivities at 25 °C of the samples with x = 0.2, 0.3 and 0.45 were 4.6×10^{-5}, 7.4×10^{-5} and 2.4×10^{-4} S cm^{-1}, respectively. It could be seen that $\log_{10}\sigma$ exhibited an almost linear dependence on the inverse temperature and therefore followed the Arrhenius equation $\sigma = \sigma_0\exp(-E_{a,DC}/(k_BT))$. The calculated activation energies $E_{a,DC}$ were 0.632, 0.590 and 0.446 eV for the samples with x = 0.3, 0.4 and 0.45, respectively. These results proved that the ionic conductivity at room temperature of cubic Li_2ZnCl_4 was greatly improved due to the solid solution formation with Li_3InCl_6. The results from equivalent circuit and DRT tests (Fig. 4b and d) show that the grain boundary resistance was the main issue in the ionic conductivity at room temperature of the sample with x = 0.45; therefore, a pellet of this sample was prepared by hot-pressing at 170 °C and 30 MPa for 1 h to reduce the grain boundary resistance. The temperature dependence of the ionic conductivity of the hot-pressed pellet is plotted in Fig. 4e and denoted as 'x = 0.45 Hot-pressed'. It could be seen that the ionic conductivity at room temperature was greatly improved because the grain boundary resistivity was reduced. The ionic conductivity at 25 °C was about 9.2×10^{-4} S cm^{-1} and the activation energy was about 0.300 eV. The ionic conductivity for x = 0.45 is comparable to that of the reported halide solid electrolytes as shown in Table 1.

Fig. 5a and b show the charge–discharge curves and cyclic properties of the prepared solid-state cell. The cells were cycled

Table 1 Summary of the ionic conductivity of some reported halide solid electrolytes

Solid electrolyte	Structure	Ionic conductivity/S cm^{-1}	Activation energy/eV	Preparation method	Ref.
Li_3YBr_6	$C2/m$	1.7×10^{-3} (RT)	0.37	Ball milling and heat treatment	5
Li_3InCl_6	$C2/m$	1.49×10^{-3} (25 °C)	—	Ball milling and heat treatment	27
Li_3InCl_6	$C2/m$	2.04×10^{-3} (25 °C)	0.347	Aqueous solution	6
Li_2ZrCl_6	$C2/m$	4.0×10^{-4} (30 °C)	0.37	Ball milling	9
Mn-doped Li_2ZrCl_6	C2/m	8.0×10^{-4} (30 °C)	0.326	Ball milling	11
$LiAlBr_4$	$P2_1/c$	1.7×10^{-4} (30 °C)	0.437	Ball milling	19
Li_3YbCl_6	$P\bar{3}m1$	1.06×10^{-4} (30 °C)	0.51	High temperature solid state reaction	28
$Li_3YBr_{5.7}F_{0.3}$	$C2/m$	2.04×10^{-3} (25 °C)	0.378	High temperature solid state reaction	29
$Li_3InCl_{4.8}F_{1.2}$	$C2/m$	5.1×10^{-4} (30 °C)	—	Ball milling and heat treatment	30
Li_3TiCl_6	$C2/m$	1.04×10^{-3} (25 °C)	0.32	Ball milling and heat treatment	18
Li_3ErI_6	$C2/c$	6.5×10^{-4} (RT)	0.37	Ball milling	17
$Li_{2.45}In_{0.45}Zn_{0.55}Cl_{4.9}$	$Fd\bar{3}m$	9.2×10^{-4} (25 °C)	0.300	Ball milling and heat treatment	This work

© 2024 The Author(s). Published by the Royal Society of Chemistry

Open Access Article. Published on 07 August 2024. Downloaded on 2/5/2026 10:04:04 AM.
This article is licensed under a Creative Commons Attribution-NonCommercial 3.0 Unported Licence.

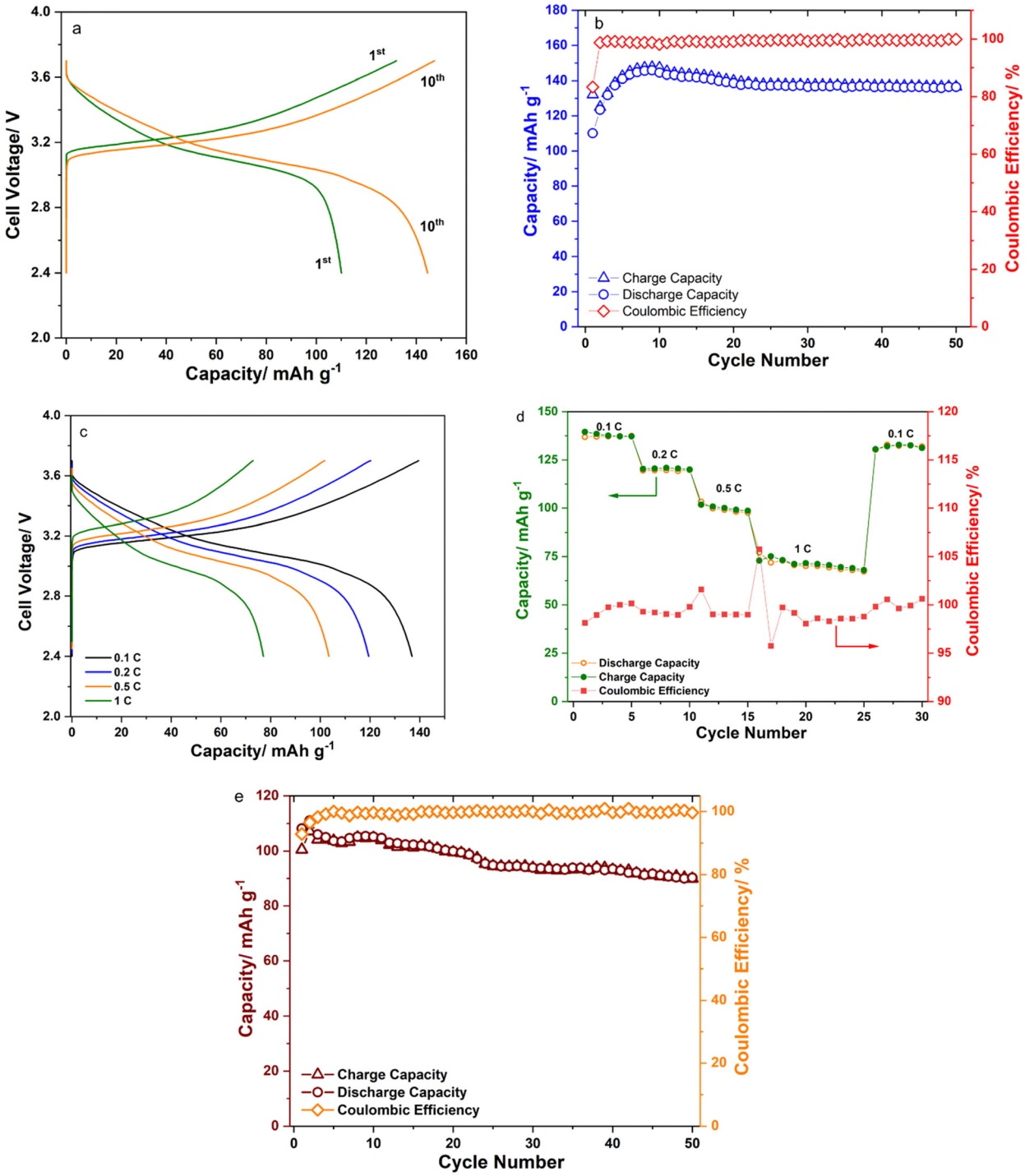

Fig. 5 (a) The 1st and 10th charge–discharge curves at 0.1C; (b) cyclic properties at 0.1C; (c) and (d) rate capability at 0.1, 0.2, 0.5 and 1C; (e) long-term cycling at 0.5C of the fabricated ASS cell.

in constant current mode at 0.1C. The initial charge–discharge capacities were 132.9 and 110.1 mA h g^{-1}_{NMC}. The charge–discharge capacities were improved and reached 147.4/144.7 mA h g^{-1}_{NMC} at the 10th cycle. The initial coulombic efficiency (CE) was about 83.6%. At the 2nd cycle, the CE was about 98.72%. From the 3rd cycle, the CE was higher than 99.5%. The cell was stable after 50 cycles and the charge–discharge capacities were still maintained at 136.6 and 136.5 mA h g^{-1}_{NMC}. The cell exhibited acceptable rate capability as shown in Fig. 5c and d. The average discharge capacities were 138, 118, 98 and 70 mA h g^{-1}_{NMC} when the cell was cycled at 0.1, 0.2, 0.5 and 1C, respectively. High reversible capacity remained after the rate performance indicated that the structure of the cell was not affected by this process. The long-term

Open Access Article. Published on 07 August 2024. Downloaded on 2/5/2026 10:04:04 AM. This article is licensed under a Creative Commons Attribution-NonCommercial 3.0 Unported Licence.

cycling at 0.5C was also investigated to study the cell's stability at a high rate. The result is shown in Fig. 5e. The cell maintained a good discharge capacity of about 90 mA h g^{-1}_{NMC} and a coulombic efficiency of about 99.8%. Thus, the results suggested that the prepared solid electrolyte was compatible with the high Ni active material $LiNi_{0.5}Mn_{0.3}Co_{0.2}O_2$.

4. Conclusion

$Li_{2+x}In_xZn_{1-x}Cl_{4+2x}$ ($0 \leq x \leq 0.5$) solid electrolytes were successfully prepared by mechanochemical synthesis. XRD results proved that the prepared samples had a cubic structure and the lattice constant was dependent on the x value. The sample with $x = 0.45$ had an ionic conductivity of about 2.4×10^{-4} S cm^{-1} at 25 °C and the grain boundary resistance was the main component of the total resistance of the sample. The hot-pressed pellet ($x = 0.45$) exhibited a decent ionic conductivity of about 9.2×10^{-4} S cm^{-1} at 25 °C and a low activation energy of about 29 kJ mol^{-1}. The all-solid-state cell was stable after 50 cycles indicating that the prepared solid electrolyte was compatible with bare $LiNi_{0.5}Mn_{0.3}Co_{0.2}O_2$.

Data availability

All the data presented in this article are present in the form of figures and tables in the manuscript itself.

Conflicts of interest

The authors declare that they have no known competing financial interests or personal relationships that could have appeared to influence the work reported in this paper.

Acknowledgements

This research received no external funding. We acknowledge Ho Chi Minh City University of Technology (HCMUT), VNU-HCM for supporting this study.

References

1 Y. Kato, S. Hori, T. Saito, K. Suzuki, M. Hirayama, A. Mitsui, M. Yonemura, H. Iba and R. Kanno, High-power all-solid-state batteries using sulfide superionic conductors, *Nat. Energy*, 2016, **1**, 16030.
2 A. Manthiram, X. Yu and S. Wang, Lithium battery chemistries enabled by solid-state electrolytes, *Nat. Rev. Mater.*, 2017, **2**, 16103.
3 Y. Zhu, X. He and Y. Mo, Origin of Outstanding Stability in the Lithium Solid Electrolyte Materials: Insights from Thermodynamic Analyses Based on First-Principles Calculations, *ACS Appl. Mater. Interfaces*, 2015, **7**, 23685–23693.
4 X. Li, J. Liang, X. Yang, K. R. Adair, C. Wang, F. Zhao and X. Sun, Progress and perspectives on halide lithium conductors for all-solid-state lithium batteries, *Energy Environ. Sci.*, 2020, **13**, 1429–1461.
5 T. Asano, A. Sakai, S. Ouchi, M. Sakaida, A. Miyazaki and S. Hasegawa, Solid Halide Electrolytes with High Lithium-Ion Conductivity for Application in 4 V Class Bulk-Type All-Solid-State Batteries, *Adv. Mater.*, 2018, **30**, e1803075.
6 X. Li, J. Liang, N. Chen, J. Luo, K. R. Adair, C. Wang, M. N. Banis, T. K. Sham, L. Zhang, S. Zhao, S. Lu, H. Huang, R. Li and X. Sun, Water-Mediated Synthesis of a Superionic Halide Solid Electrolyte, *Angew. Chem., Int. Ed.*, 2019, **58**, 16427–16432.
7 K. Tuo, C. Sun and S. Liu, Recent Progress in and Perspectives on Emerging Halide Superionic Conductors for All-Solid-State Batteries, *Electrochem. Energy Rev.*, 2023, **6**, 17.
8 X. Nie, J. Hu and C. Li, Halide-based solid electrolytes: The history, progress, and challenges, *Interdiscip. Mater.*, 2023, **2**, 365–389.
9 H. Kwak, D. Han, J. Lyoo, J. Park, S. H. Jung, Y. Han, G. Kwon, H. Kim, S. T. Hong, K. W. Nam and Y. S. Jung, New Cost-Effective Halide Solid Electrolytes for All-Solid-State Batteries: Mechanochemically Prepared Fe^{3+}-Substituted Li_2ZrCl_6, *Adv. Energy Mater.*, 2021, **11**, 202003190.
10 H. Kwak, D. Han, J. P. Son, J. S. Kim, J. Park, K.-W. Nam, H. Kim and Y. S. Jung, Li+ conduction in aliovalent-substituted monoclinic Li2ZrCl6 for all-solid-state batteries: $Li_{2+x}Zr_{1-x}M_xCl_6$ (M = In, Sc), *Chem. Eng. J.*, 2022, **437**, 135413.
11 H.-J. Jeon, Y. Subramanian and K.-S. Ryu, Variation of electrochemical performance of Li_2ZrCl_6 halide solid electrolyte with Mn substitution for all-solid-state batteries, *J. Power Sources*, 2024, **602**, 234343.
12 L. Zhou, C. Y. Kwok, A. Shyamsunder, Q. Zhang, X. Wu and L. F. Nazar, A new halospinel superionic conductor for high-voltage all solid state lithium batteries, *Energy Environ. Sci.*, 2020, **13**, 2056–2063.
13 N. Tanibata, S. Takimoto, K. Nakano, H. Takeda, M. Nakayama and H. Sumi, Metastable Chloride Solid Electrolyte with High Formability for Rechargeable All-Solid-State Lithium Metal Batteries, *ACS Mater. Lett.*, 2020, **2**, 880–886.
14 J. Park, D. Han, H. Kwak, Y. Han, Y. J. Choi, K.-W. Nam and Y. S. Jung, Heat treatment protocol for modulating ionic conductivity via structural evolution of $Li_{3-x}Yb_{1-x}M_xCl_6$ (M = Hf^{4+}, Zr^{4+}) new halide superionic conductors for all-solid-state batteries, *Chem. Eng. J.*, 2021, **425**, 130630.
15 J. Liang, X. Li, K. R. Adair and X. Sun, Metal Halide Superionic Conductors for All-Solid-State Batteries, *Acc. Chem. Res.*, 2021, **54**, 1023–1033.
16 J. L. Changhong Wang, J. Tae Kim and X. Sun, Prospects of halide-based all-solid-state batteries: From material design to practical application, *Sci. Adv.*, 2022, **8**, eadc9516.
17 R. Schlem, T. Bernges, C. Li, M. A. Kraft, N. Minafra and W. G. Zeier, Lattice Dynamical Approach for Finding the Lithium Superionic Conductor Li_3ErI_6, *ACS Appl. Energy Mater.*, 2020, **3**, 3684–3691.
18 K. Wang, Z. Gu, Z. Xi, L. Hu and C. Ma, Li_3TiCl_6 as ionic conductive and compressible positive electrode active material for all-solid-state lithium-based batteries, *Nat. Commun.*, 2023, **14**, 1396.

© 2024 The Author(s). Published by the Royal Society of Chemistry

Open Access Article. Published on 07 August 2024. Downloaded on 2/5/2026 10:04:04 AM.
This article is licensed under a Creative Commons Attribution-NonCommercial 3.0 Unported Licence.

19 N. Flores-Gonzalez, N. Minafra, G. Dewald, H. Reardon, R. I. Smith, S. Adams, W. G. Zeier and D. H. Gregory, Mechanochemical Synthesis and Structure of Lithium Tetrahaloaluminates, $LiAlX_4$ (X = Cl, Br, I): A Family of Li-Ion Conducting Ternary Halides, *ACS Mater. Lett.*, 2021, **3**, 652–657.

20 K. Wussow, P. Kuske and H. D. Lutz, Ionic Conductivity, Structural, IR and Raman Spectroscopic Data of Olivine, Sr_2PbO_4, and Na_2CuF_4 Type Lithium and Sodium Chlorides Li_2ZnCl_4 and Na_2MCl_4 (M = Mg, Ti, Cr, Mn, Co, Zn, Cd), *Z. Naturforsch., B*, 2014, **42**, 1379–1386.

21 T. Y. Kanno Ryoji, Mori Masashi and Yamamoto Osamu, Ionic Conductivity and Structure of Double Chloride Li_2ZnCl_4 in the LiCl–$ZnCl_2$ System, *Chem. Lett.*, 1989, 223–226.

22 H. Gamo, N. Huu Huy Phuc, M. Ikari, K. Hikima, H. Muto and A. Matsuda, Electrochemical redox of Li_2S–CaS and –CaX_2 (X = Cl, Br, and I) cathode materials for all-solid-state lithium-sulfur batteries, *Electrochim. Acta*, 2022, **431**, 141149.

23 N. H. H. Phuc, K. Morikawa, T. Mitsuhiro, H. Muto and A. Matsuda, Synthesis of plate-like Li_3PS_4 solid electrolyte via liquid-phase shaking for all-solid-state lithium batteries, *Ionics*, 2017, **23**, 2061–2067.

24 P. Molaiyan, S. E. Mailhiot, K. Voges, A. M. Kantola, T. Hu, P. Michalowski, A. Kwade, V.-V. Telkki and U. Lassi, Investigation of the structure and ionic conductivity of a Li_3InCl_6 modified by dry room annealing for solid-state Li-ion battery applications, *Mater. Des.*, 2023, **227**, 111690.

25 J. B. Nelson and D. P. Riley, An experimental investigation of extrapolation methods in the derivation of accurate unit-cell dimensions of crystals, *Proc. Phys. Soc.*, 1945, **57**, 160–177.

26 T. H. Wan, M. Saccoccio, C. Chen and F. Ciucci, Influence of the Discretization Methods on the Distribution of Relaxation Times Deconvolution: Implementing Radial Basis Functions with DRT tools, *Electrochim. Acta*, 2015, **184**, 483–499.

27 X. Li, J. Liang, J. Luo, M. Norouzi Banis, C. Wang, W. Li, S. Deng, C. Yu, F. Zhao, Y. Hu, T.-K. Sham, L. Zhang, S. Zhao, S. Lu, H. Huang, R. Li, K. R. Adair and X. Sun, Air-stable Li_3InCl_6 electrolyte with high voltage compatibility for all-solid-state batteries, *Energy Environ. Sci.*, 2019, **12**, 2665–2671.

28 S. Y. Kim, K. Kaup, K.-H. Park, A. Assoud, L. Zhou, J. Liu, X. Wu and L. F. Nazar, Lithium Ytterbium-Based Halide Solid Electrolytes for High Voltage All-Solid-State Batteries, *ACS Mater. Lett.*, 2021, **3**, 930–938.

29 T. Yu, J. Liang, L. Luo, L. Wang, F. Zhao, G. Xu, X. Bai, R. Yang, S. Zhao, J. Wang, J. Yu and X. Sun, Superionic Fluorinated Halide Solid Electrolytes for Highly Stable Li-Metal in All-Solid-State Li Batteries, *Adv. Energy Mater.*, 2021, **11**, 202101915.

30 S. Zhang, F. Zhao, S. Wang, J. Liang, J. Wang, C. Wang, H. Zhang, K. Adair, W. Li, M. Li, H. Duan, Y. Zhao, R. Yu, R. Li, H. Huang, L. Zhang, S. Zhao, S. Lu, T. K. Sham, Y. Mo and X. Sun, Advanced High-Voltage All-Solid-State Li-Ion Batteries Enabled by a Dual-Halogen Solid Electrolyte, *Adv. Energy Mater.*, 2021, **11**, 202100836.